Nanomedicine: Nanotechnology, Biology, and Medicine
xx (2017) xxx–xxx

nanomedicine
Nanotechnology, Biology, and Medicine

nanomedjournal.com

Special Topic: Two-Dimensional Biomaterials in Regenerative Medicine

Sculpting neurotransmission during synaptic development by 2D nanostructured interfaces

Niccolò Paolo Pampaloni[a], Denis Scaini[b,c,*], Fabio Perissinotto[b,c], Susanna Bosi[d], Maurizio Prato[d,e,f,**], Laura Ballerini[a,***]

[a]*International School for Advanced Studies (SISSA), Trieste, Italy*
[b]*Life Science Department, University of Trieste, Trieste, Italy*
[c]*ELETTRA Synchrotron Light Source, Trieste, Italy*
[d]*Department of Chemical and Pharmaceutical Sciences, University of Trieste, Trieste, Italy*
[e]*Basque Foundation for Science, Ikerbasque, Bilbao, Spain*
[f]*CIC BiomaGUNE, Parque Tecnológico de San Sebastián, San Sebastián (Guipúzcoa), Spain*

Received 4 August 2016; accepted 4 January 2017

Abstract

Carbon nanotube-based biomaterials critically contribute to the design of many prosthetic devices, with a particular impact in the development of bioelectronics components for novel neural interfaces. These nanomaterials combine excellent physical and chemical properties with peculiar nanostructured topography, thought to be crucial to their integration with neural tissue as long-term implants. The junction between carbon nanotubes and neural tissue can be particularly worthy of scientific attention and has been reported to significantly impact synapse construction in cultured neuronal networks. In this framework, the interaction of 2D carbon nanotube platforms with biological membranes is of paramount importance. Here we study carbon nanotube ability to interfere with lipid membrane structure and dynamics in cultured hippocampal neurons. While excluding that carbon nanotubes alter the homeostasis of neuronal membrane lipids, in particular cholesterol, we document in aged cultures an unprecedented functional integration between carbon nanotubes and the physiological maturation of the synaptic circuits.

Key words: Nanostructured materials; Patch clamp; Cholesterol; Synaptic release; Vesicle pools

Neurons are continuously exposed to signals generated by the extracellular environment, including genuine physical cues (such as mechanical or topographical ones) at the nanoscale, able to drive key biological tasks.[1] This ability has been exploited to engineer interfaces with nanostructures with the aim of guiding nerve tissue re-growth.[2–4] Varied strategies have been adopted to decorate bio-interfaces with nano-features[5,6] and incorporating nanomaterials has emerged as a promising one.[5,6] Conductive nanomaterials, such as carbon nanotubes, have received particular attention[7–9] and were shown, when used to interface cultured neurons, to improve the growth of axons[10,11] and to enhance the construction of synaptic connections between

Abbreviations: AFM, atomic force microscopy; CT-B, Cholera Toxin subunit-B; DIV, days in vitro; DOPC, 1,2-Dioleoyl-sn-glycero-3-phosphocholine; MβCD, Methyl-β-Cyclodextrin; mPSCs, miniature post-synaptic currents; MWCNTs, multi-walled carbon nanotubes; PSCs, post-synaptic currents; SLM, artificial lipid membranes; SPM, scanning probe microscopy; TTX, Tetrodotoxin; VGLUT1, vesicular glutamate transporter 1

Financial supports from: This work was supported by the ByAxon n. 737116, NEUROSCAFFOLDS-FP7-NMP-604263 and the PRIN-MIUR n. 2012MYESZW to L.B.

Competing interests: The Authors declare no competing financial interests.

Authors' contributions: NPP performed electrophysiology, immunocytochemistry and confocal microscopy experiments and contributed to the analysis. DS and FP performed SLM experiments and AFM analysis. SB and MP provided the materials. LB and DS conceived the idea and designed the experiments. LB and DS wrote the manuscript. LB provided funding. All authors read and approved the final manuscript.

*Correspondence to: D. Scaini, Life Science Department, University of Trieste, Trieste, Italy.
**Correspondence to: M. Prato, Department of Chemical and Pharmaceutical Sciences, University of Trieste, Trieste, Italy.
***Corresponding author.
E-mail addresses: npampalo@sissa.it (N.P. Pampaloni), dscaini@sissa.it (D. Scaini), fabio.perissinotto@elettra.eu (F. Perissinotto), sbosi@units.it (S. Bosi), prato@units.it (M. Prato), laura.ballerini@sissa.it (L. Ballerini).

http://dx.doi.org/10.1016/j.nano.2017.01.020

neurons.[12–15] More precisely, the extracellular environment, when artificially reconstructed by multi-walled carbon nanotubes (MWCNTs), induced synaptogenesis in cultured hippocampal neurons during early network formation.[12,15,16] Enhancing cell-to-cell communication is crucial in neural circuits' settings,[17] however the role and dynamics of the interactions between MWCNTs and the cellular surfaces (the "nano-bio" interface[18]) are largely unexplored.

The majority of current studies on biological membrane stability in response to nanomaterials are focused on the influence of materials' functionalization or shape/size on cell uptake mechanisms and internalization, to engineer sophisticated drug delivery (nano)-vectors.[19] In this framework, neuronal membranes have been shown to recover even when transiently pierced or deformed by (nano)needles[20] or other intracellular (nano) delivery systems.[21] Water-soluble single-walled carbon nanotubes grafted to poly ethylene glycol impaired, when added to the culturing medium, membrane re-cycling in neurons, presumably by affecting the endocytosis of released vesicles at the pre-synaptic site.[22] However, more specific information about neuronal membrane stability when chronically interfaced to pristine nanomaterial-based growth substrates is lacking. Cell membranes are directly exposed to MWCNTs,[14,23] but there are no reports on the effects that MWCNT interfaces exert on neuronal membrane equilibrium. Recent studies targeted the interaction between lipoid membranes and MWCNTs in suspension.[24,25] Molecular simulations showed that significant changes in the structure of individual lipid molecules, and in their two-dimensional packing, were observed when MWCNTs were adsorbed on cell membranes and subsequently pierced the lipid bilayer.[26,27]

Here, by single cell electrophysiology and immunofluorescence microscopy we monitor the dynamics of glutamate receptor-mediated excitatory transmission in cultured hippocampal neurons interfaced to MWCNTs. We specifically addressed whether MWCNTs, once interfaced to neurons, affected synaptic transmission by modulating lipid membrane structure and dynamics. We focused in particular on cholesterol, a largely represented lipid in neuronal membranes known to regulate presynaptic vesicle release.[28,29] For a first general assessment we used artificial lipid membranes that, when interfaced to MWCNTs, were more stable, in respect to controls, to a cholesterol depleting-agent, i.e. cyclodextrin.[30] Conversely, in cultured neurons, MWCNT interfaces did not alter the membrane cholesterol distribution neither prevented its subsequent depletion by cyclodextrin. Unexpectedly, by cholesterol removal, we unmasked MWCNT ability to shape pre-synaptic vesicle populations at newly formed glutamatergic connections. Finally, we followed up the effects of long term MWCNT interfacing in neural synaptic networks.

Methods

Synthesis of MWCNTs

MWCNTs 20-30 nm in diameter (Nanostructured & Amorphous Materials, Inc.) were used as received and substrates were prepared as described previously.[12,15] Briefly, MWCNT 20-30 nm were functionalized using 1,3-dipolar cycloaddition with heptanal and sarcosine at 130 °C for 120 h in dimethylformammide (DMF) as solvent. For deposition on the coverslips, the DMF solution of functionalized MWCNTs (0.01 mg/mL) was drop casted to uniformly layer the entire substrate and let evaporated at 80 °C, then, the substrates were heated up at 350 °C under N_2 atmosphere to induce the complete re-pristinization of MWCNTs. The uniformity of the deposition was assumed by AFM (Figure 1, *B*) and by scanning electron microscopy (SEM, in Supplementary Figure S1, *D*).

Artificial membrane preparation and characterization

Artificial membranes were prepared by lipid spreading on a supporting glass slide from an organic solvent solution. 1,2-Dioleoyl-sn-glycero-3-phosphocholine (DOPC) and cholesterol molecules (both from Avanti Polar Lipids Inc., US) were dissolved in a 2:1 ratio in chloroform (Sigma Aldrich) at a final concentration of 100 μM. 100 μL of solution were deposited on a glass coverslip, used as control, and on MWCNTs substrates supported by the same glass coverslip (Figure 1).[15] Samples were settled at 37 °C, 80% UR for 30 min, then rinsed in mQ water, dried with a gentle flow of N_2 and mounted on metallic plates using epoxy glue for subsequent atomic force microscopy (AFM) imaging (MFP-3D™, Asylum Research, Santa Barbara, CA, U.S.). Measurements were carried out in buffer solution (HEPES, Sigma Aldrich) at room temperature (RT, 18 to 22 °C) working in dynamic mode. Cantilevers, characterized by a resonant frequency of 69 kHz and force constant of 0.39 nN/nm (OMCL-RC800PSA-1 tips from Olympus Co., Japan), were used working at low oscillation amplitudes with half free-amplitude set-point. Images were acquired at 512 × 512 pixels at 0.75 lines/s scan speed. Artificial membranes for fluorescence experiments were prepared following the same procedure described above but DOPC molecules were mixed with 2% of fluorescent lipid (18:1-06:0 NBD PC, from Avanti Polar Lipids Inc., US). Fluorescent measurements were done by epifluorescence microscopy (Eclipse Ti-U, Nikon Co., Japan; 20× objective, 0.45 NA). Samples were mounted in a liquid cell and the decay in fluorescent signal from both membranes deposited on control and MWCNT substrates were recorded for 60 min after injection of 500 μM Methyl-β-Cyclodextrin (MβCD, Sigma Aldrich) to deplete cholesterol.[30] Decay plots are the average of 3 independent experiments. Values were normalized to the fluorescent signal immediately before MβCD injection. AFM images were analyzed using Gwyddion, open-source modular program for scanning probe microscopy (SPM) data visualization and analysis.[31] Surface roughness was determined as RMS value of the height irregularities on 2.5 μm^2 membrane area. Decays were fitted using a double exponential function using Igor Pro software (Wavemetrics, US). Figure S1, *C* shows the amplitude (error) AFM images of the high magnification reconstructions shown in Figure 1, *A-C*.

Raman characterization

The Raman measurements were performed in the reflection geometry. A 532 nm continuous-wave laser (Cobolt Samba,

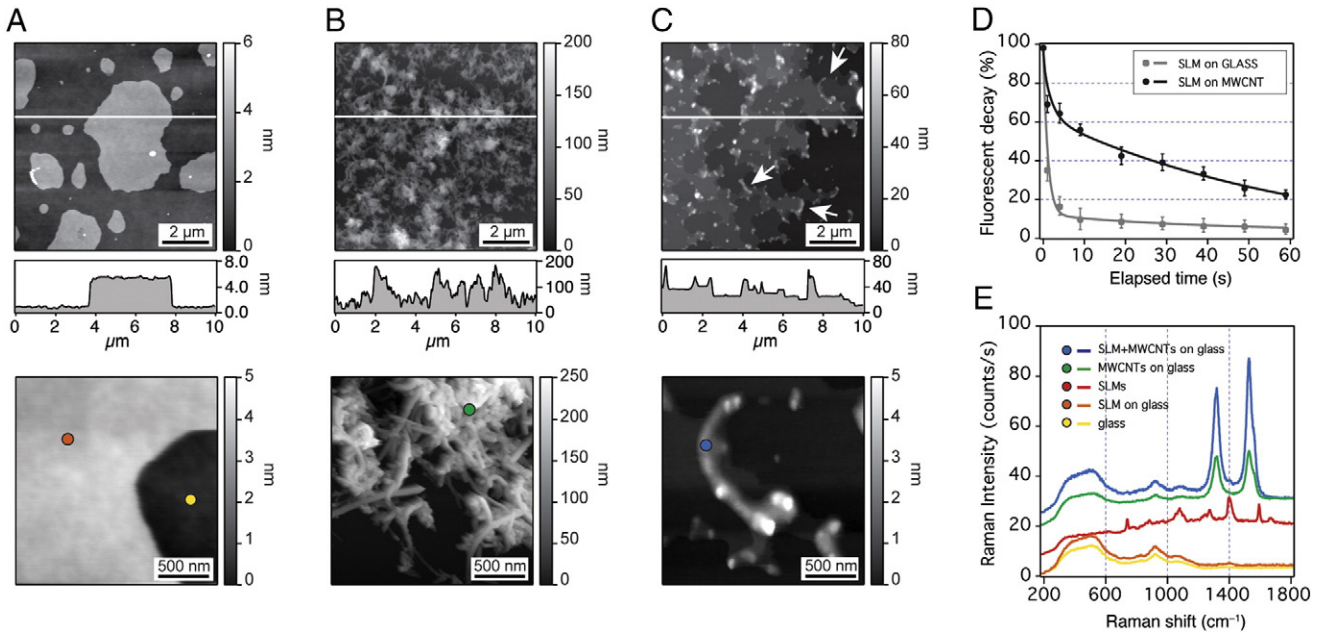

Figure 1. AFM investigation of artificial lipid membranes (SLM). **(A)** Low magnification topographic reconstruction of an incomplete SLM deposited on a control glass surface (on the top). The height profile corresponding to the highlighted line is shown, revealing SLM height of about 5.0 ± 0.2 nm. Higher resolution AFM reconstruction (on the bottom) demonstrates the high uniformity of the so obtained SLB. B. Low magnification topographic reconstruction, corresponding height profile and higher resolution reconstruction of a MWCNTs carpet deposited on glass via drop-casting. Note the high corrugation of the resulting surface pointed out by the top image and single MWCNTs composing the carpet easily distinguishable in the bottom one. **(C)** Low magnification topographic reconstruction, corresponding height profile and higher resolution reconstruction of SLBs deposited on a MWCNTs substrate. It is possible to appreciate (white arrows) MWCNT ability to pierce SLMs, indicated by nanotubes emerging from the upper membrane layer. The altimetric profile reveals flat parts, corresponding to superficial SLBs, from which only MWCNTs apexes protrude. **(D)** Fluorescent decay of SLMs signal after injection of MβCD (500 μM) detected in control (squares) and on MWCNT (circles) membranes. Note that the decay follows a double exponential law characterized by τ values of 1.09 ± 0.02 s and 39.02 ± 9.83 s (gray fitting line) for SLM deposited on glass and 2.02 ± 0.15 s and 63.67 ± 6.92 s for SLM deposited on the MWCNT carpet (black fitting line). Data are averages of 3 independent experiments expressed as mean ± SD. Initial values were normalized before injection of MβCD. E. Raman spectra acquired in the highlighted areas (colored dots) in the bottom panels of A, B and C (glass substrate in yellow, SLM on glass in orange, MWCNTs on glass in green and SLM above MWCNTs in blue). Note that the spectra of MWCNTs with (blue spectrum) and without (green spectrum) SLMs were vertically shifted for illustrative purpose. The reference spectrum of lipids (red spectrum) was acquired on a many-layer membranes sample (MLMs, not shown) in order to minimize Raman signal from the underlying glass surface.

50 mW, bandwidth 1 MHz) was used as excitation source. The beam was focused on the sample by a 100× air objective (NA 0.8, EC EpiPlan, Zeiss) resulting in a diameter of laser spot of about 0.5 μm. A 532 nm RazorEdge Dichroic™ laser-flat beam-splitter and a 532 nm RazorEdge® ultra-steep long-pass edge filter were used to direct the light into microscope and cut Rayleigh scattered light, respectively. The laser power on the sample was controlled by the neutral density filter (Thorlabs) and kept at 100 μW. The acquisition time in all experiments was 60 s. All Raman measurements and analysis were performed by CNR-IOM (TASC Laboratory, Basovizza, Trieste, Italy).

Primary cultures and cell treatment

Hippocampal neurons were obtained from neonatal rats as previously reported.[15] Cells were plated on poly-L-ornithine-coated (Sigma Aldrich) or on MWCNT-coated glass coverslips and incubated at 37 °C, 5% CO_2 in culture medium. Cultured cells were used for experiments either at 8 to 10 and 18 to 21 days in vitro (DIV). To deplete cholesterol from neuronal membranes, cultures were incubated with 1 mM MβCD (Sigma Aldrich) for 1 h at 37 °C.[30] MβCD is a cyclic glucose oligomer with a hydrophobic cavity that is able to bind lipids (especially cholesterol) and make them water-soluble[32] and is commonly used to deplete membrane cholesterol acutely from both leaflets of the bilayer.[33]

Electrophysiology

Patch-clamp, whole cell recordings were obtained with glass micropipettes with a resistance of 4 to 8 MΩ. The intracellular pipette solution was the following (mM): 120 K gluconate, 20 KCl, 10 HEPES, 10 EGTA, 2 $MgCl_2$, 2 Na_2ATP, pH 7.3. The external standard saline solution contained (mM): 150 NaCl, 4 KCl, 1 $MgCl_2$, 2 $CaCl_2$, 10 HEPES, 10 glucose, pH 7.4. All recordings were performed at RT. Cells were voltage clamped at a holding potential set at −56 mV (not corrected for the liquid junction potential, calculated to be 13.7 mV at 20 °C). The uncompensated series resistance had values <8 MΩ. Miniature post-synaptic currents (mPSCs) were recorded in the presence of 1 μM fast-Na^+ channel blocker Tetrodotoxin (TTX; Latoxan). In order to block voltage-gated calcium channels we added 3 mM $CoCl_2$ to the external solution. Data were collected using a Multiclamp 700A Amplifier (Molecular Devices, US), and

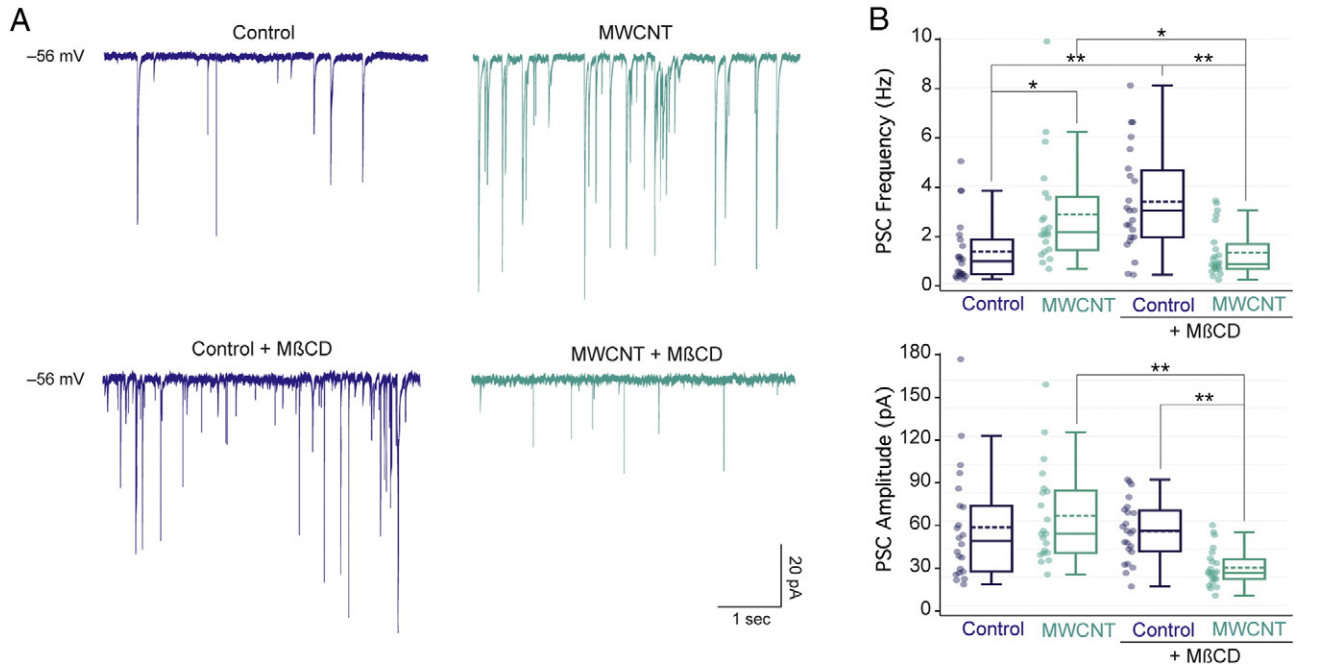

Figure 2. Cholesterol removal by MβCD application in hippocampal cultures. **(A)** Representative traces of spontaneous synaptic activity in control (left) and MWCNT (right) neurons before (top) and after (bottom) MβCD application. **(B)** Box plots summarize pooled data of PSC frequencies (top) and amplitudes (bottom) recorded from control and MWCNTs neurons prior and after MβCD. Note the higher PSC frequency displayed by MWCNT neurons in standard saline and the opposite effects brought about by MβCD in control and MWCNTs.

analyzed using either Clampfit 10.3 (Molecular Devices) or Axograph (Axograph Scientific). Glutamate AMPA-receptor and $GABA_A$-receptor mediated post synaptic currents (PSCs) were isolated offline by building two templates with different kinetic parameters: respectively 0.1 ms rise-time; 3 and 30 ms decay time constant (τ); 10 and 100 ms template length. Previous work[12,15] indicated that in our experimental conditions, the vast majority of fast-decaying ($\tau < 5$ ms) PSCs are mediated by the glutamate AMPA-receptor type; while the slow-decaying ($\tau > 20$ ms) PSCs are mediated by the $GABA_A$-receptor type.

Immunocytochemistry

Cultures were fixed in 4% formaldehyde (prepared from fresh paraformaldehyde) in PBS for 20 min, permeabilized with 0.3% Triton-X-100 and subsequently incubated with primary antibodies for 30 min at RT and after washing in PBS incubated with secondary antibodies for 45 min. Cultures were then mounted with the *Vectashield* (Vector Laboratories) on 1 mm thick microscope glass slides. To visualize neurons and lipid rafts we used the following: rabbit anti-β-tubulin III primary antibody (Sigma T2200, 1:250 dilution) and Alexa 594 goat anti rabbit secondary antibody (Invitrogen, 1:500); Alexa 488 Cholera Toxin subunit-B (CT-B) 1:200 (Molecular Probes) and DAPI, 1:1000 (Invitrogen).

To visualize glutamatergic synapses we co-label neurons with the guinea pig anti-vesicular glutamate transporter 1 (VGLUT1; Millipore, 1:2000) and β-tubulin III (Sigma, 1:250) primary antibodies and Alexa 594 goat anti rabbit (Invitrogen, 1:500) and Alexa 488 goat anti guinea-pig (Invitrogen, 1:500) as secondary antibodies. All images were acquired using an inverted confocal Microscope (Leica Microsystems GmbH, Wetzlar, Germany; 40× oil immersion objective, 1.25 NA).

To quantify VGLUT1 puncta and lipid rafts, n = 20 ± 10 z-stacks (acquired every 0.4 μm) were taken from n = 10 randomly selected fields (240 μm × 240 μm) per coverslip (n = 30, 3 culture series in Control and MWCNTs). To quantify lipid rafts, we selected the CT-B positive objects (<5 μm^3) co-localized to the β-tubulin III positive areas. For each image, the volumes of CT-B positive objects were normalized to the β-tubulin III positive volumes. To quantify VGLUT1 puncta, we selected only VGLUT1-positive puncta (<2 μm3) co-localized to the β-tubulin III positive areas and puncta were normalized to the β-tubulin III positive volumes. Images were analyzed using the Volocity software (Perkin Elmer).

For the filipin labeling of membrane cholesterols[34] cells were fixed, rinsed in PBS and directly incubated for 2 h at RT with 0.05 mg/mL filipin (Sigm-F9765) then mounted and imaged with an Epifluorescence Microscope (DM 6000, Leica; 40× objective, 0.75 NA). We collected 10 fields (355 μm × 265 μm) per coverslip (n = 30, 3 culture series for control and MWCNT) with the same CCD exposure time and illumination intensity. For each image the background fluorescence was subtracted and the fluorescence of four equal squared areas was determined. The average of these four values represented the fluorescence intensity value for each image.[34] Fluorescence signals were quantified using ImageJ software (http://rsb.info.nih.gov/ij/).

Data analysis

All values from samples subjected to the same experimental protocols were pooled together and expressed as mean ± SEM

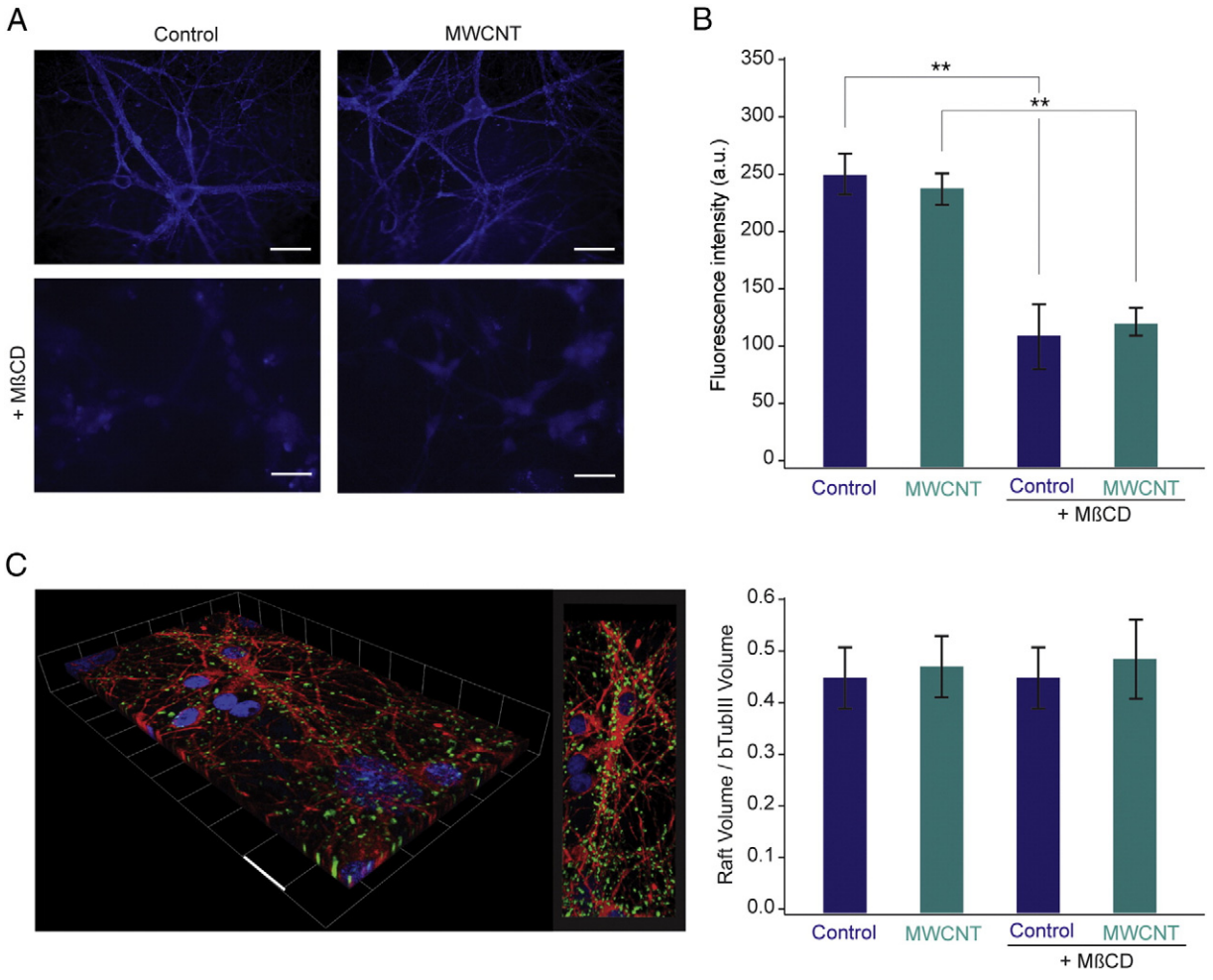

Figure 3. MβCD efficiently removed membrane cholesterol without disrupting lipid rafts. **(A)** Fluorescence micrographs of control and MWCNT hippocampal cells labeled by filipin prior (top) and after (bottom) MβCD treatment. Scale bars 50 μm. **(B)** Bar plot of filipin-derived fluorescence intensity in cultured neurons, note the similar values between control and MWCNT conditions and the comparable reduction upon cholesterol depletion by MβCD. **(C)** Left, 3D and 2D confocal reconstructions of hippocampal cultures immune-labeled with the neuronal marker β-tubulin III (in red) and the lipid-raft marker CT-B (in green), in blue DAPI labeling for nuclei. Scale bars 15 μm. Right, bar plot quantifies the CT-B volume in respect to the β-tubulin III one, note that no differences were observed between controls and MWCNTs before and after the MβCD treatment.

(with n = number of cells, unless otherwise indicated). A statistically significant difference between data sets was assessed by one-way and two-way ANOVA, followed by Bonferroni test. Statistical significance was determined at $P < 0.05$, unless otherwise indicated. Box plots were created using Plotly software (https://plot.ly).

Ethical statement

All animal procedures were conducted in accordance with the National Institutes of Health and with international and institutional standards for the care and use of animals in research, and after consulting with a veterinarian. All experiments were performed in accordance with European Union (EU) guidelines (2010/63/UE) and Italian law (decree 26/14) and were approved by the local authority veterinary service and by our institutional (SISSA-ISAS) ethical committee. All efforts to minimize animal suffering and to reduce the number of animals used were made. Animal use was approved by the Italian Ministry of Health, in agreement with the EU Recommendation 2007/526/CE (http://eur-lex.europa.eu/legal-content/EN/TXT/?uri=uriserv:OJ.L_.2007.197.01.0001.01.ENG&toc=OJ:L:2007:197:TOC).

Results

Artificial lipid membranes interfaced to MWCNTs

In the first set of experiments, we investigated by AFM the appearance of artificial lipid membranes (SLM)[35] interfaced to control substrates or to MWCNTs (Figure 1, *B*; see also[15]). SLM islands grown on control glass coverslips (Figure 1, *A*) and on MWCNTs (Figure 1, *C*) displayed similar morphology (SLM surface roughness 0.38 nm and 0.44 nm when formed on glass and on MWCNT, respectively, Figure 1, *A-C*), however AFM revealed the ability of MWCNTs to pierce membrane layers through SLM entire thickness (Figure 1, *C*, white arrows). These cross interactions induced the occasional appearance of localized

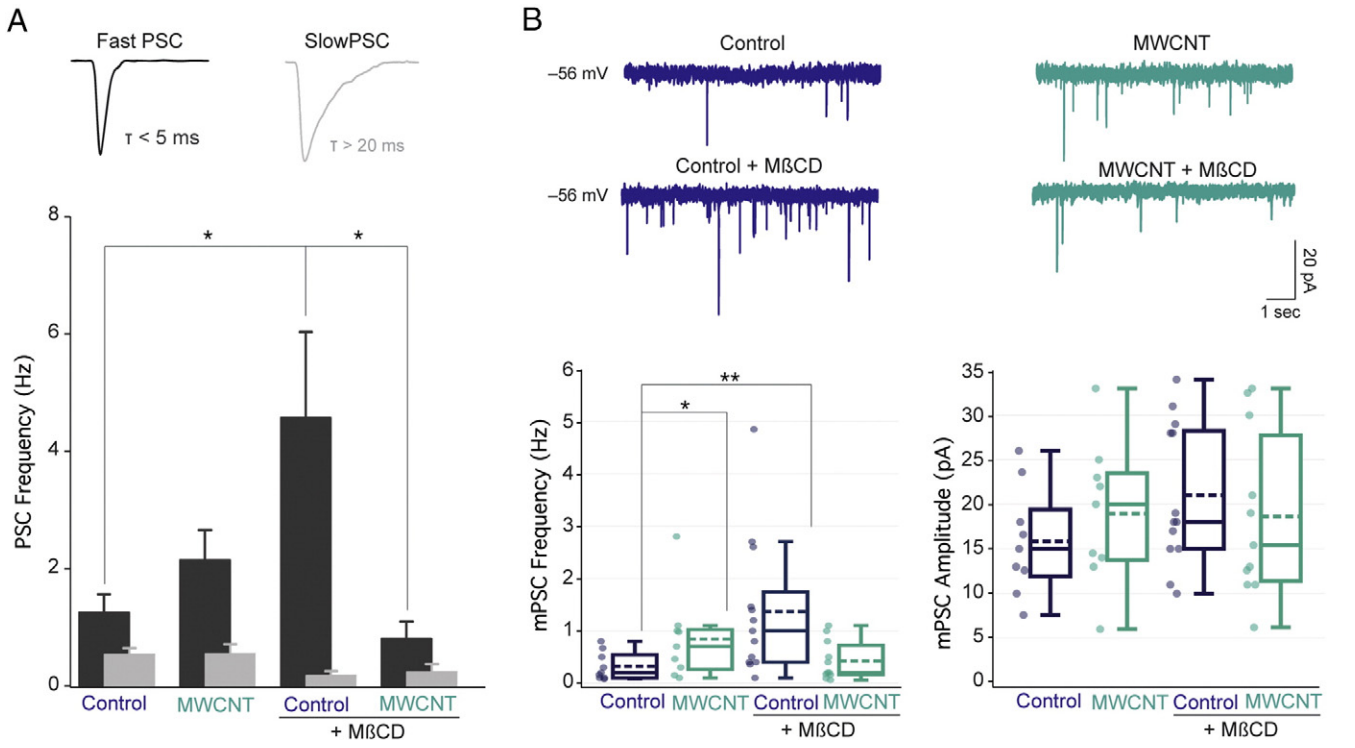

Figure 4. Depletion of cholesterol with MβCD alters fast PSCs occurrence. **(A)** Offline differential analysis of PSC decays (τ) identifies fast and slow events (insets average tracings from the same neurons as in Figure 2, *A*) both in control and MWCNTs. Bar plot summarizes the frequency of fast and slow PSCs in controls and MWCNTs. **(B)** Spontaneous synaptic activity recorded in the presence of TTX; controls and MWCNT mPSC frequency and amplitudes are summarized in the box plots before and after MβCD treatment. Note that mPSC amplitude values are unaffected.

areas where several layers of SLM piled on the surface, due to MWCNTs, a condition rarely observed in controls (Figure 1, *A* and *C*, compare the height profiles).

In Figure 1, *E* the reference Raman spectrum of lipids (in red) is plotted and is characterized by peaks associated with C–N stretch (715 cm^{-1}), C–C stretch (1090 cm^{-1}), CH_2 deformation (1305 cm^{-1} and 1440 cm^{-1}), and C = C stretch (1655 cm^{-1}) vibrations.[36,37] The Raman spectrum of MWCNTs alone on glass substrate (Figure 1, *E*, in green) shows two broad peaks centered at 1350 cm^{-1} and 1590 cm^{-1} that are commonly assigned to the presence of disorder in graphitic materials and to the tangential vibrations of the carbon atoms, respectively.[38,39] The distinguishable shoulder at 1620 cm^{-1} is a double-resonance Raman feature induced by disorder, defects or ion intercalation between the graphitic walls.[38] When SLMs are deposited on glass substrate (Figure 1, *E*, in orange), the strong contribution of the underneath glass is evident, however the lipid peak at 1440 cm^{-1} (CH_2 deformation) is distinguishable in spite of the lower amount of lipids forming the SLM. In SLM on MWCNTs, the characteristic two peaks at 1350 cm^{-1} and 1590 cm^{-1} present on the tubular structures protruding from SLMs (depicted in Figure 1, *C*, bottom panel) confirm that they are MWCNTs, as suggested by the AFM morphology. Interestingly, in this spectrum (in blue in Figure 1, *E*), the peak at 715 cm^{-1} is evident as well. This may be due to the larger laser spot diameter (about 500 nm) compared with MWCNTs (50-250 nm), resulting in a contribution of the surrounding SLBs in the Raman spectrum. Note that broad peaks observed at 400 cm^{-1} and 900 cm^{-1} are due to a photoluminescence in glass substrate, a well-known phenomenon when using a 532 nm excitation wavelength.[40]

Next, we incorporated a fluorescent lipid to SLMs (see Methods) and we compared the efficacy of MβCD treatment (500 μM; 1 h; used to bind and extract cholesterol from the membrane[32,33]) in depleting cholesterol in control and MWCNT SLMs. The plot in Figure 1, *D* summarizes the decay in fluorescence monitored during MβCD application. In order to have comparable measurements, we sampled single SLM layers in both groups. In MWCNTs, SLM lipids appeared more stabilized, as indicated by their significantly slower depletion with respect to controls (decay time constant (τ) average values: $\tau_1 = 1.09 \pm 0.02$ s and $\tau_2 = 39.02 \pm 9.83$ s for control SLMs; $\tau_1 = 12.02 \pm 0.15$ s and $\tau_2 = 63.67 \pm 6.92$ s for SLM deposited on MWCNTs; $P < 0.01$ for τ_1 values; $P < 0.05$ for τ_2; n = 3 different samples each group).

Such results suggest that interfacing with MWCNTs might affect lipid, in particular cholesterol, dynamics in biological membranes.

Acute cholesterol removal in control and MWCNTs hippocampal cultures

To further explore the potential role of MWCNTs in membrane lipid dynamics when interfacing living cells, and in particular in altering cholesterol homeostasis in neurons, we cultured hippocampal cells on control substrates or on meshworks of MWCNTs

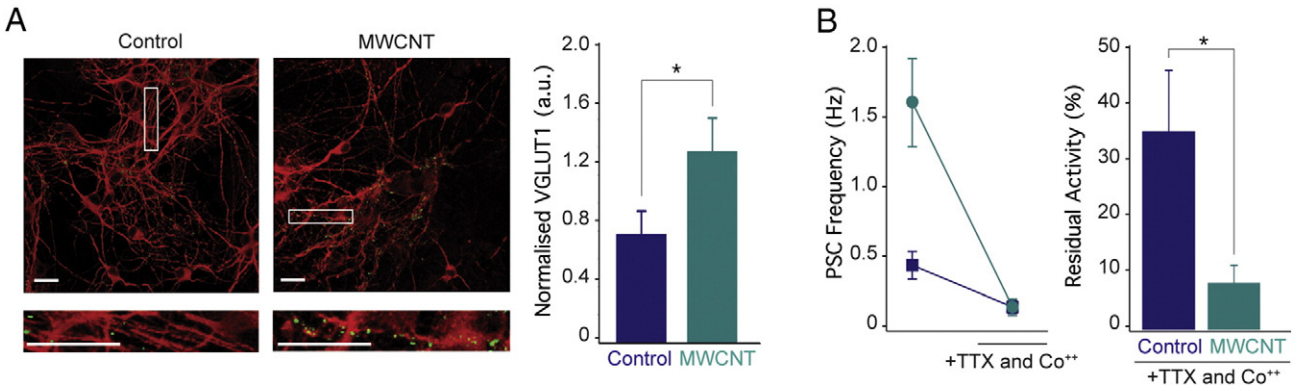

Figure 5. Co-localization of VGLUT1 and β-tubulin III immunostaining in control and MWCNT hippocampal cultures. **(A)** Right, confocal images of hippocampal neurons at 8-10 DIV stained for β-tubulin III (in red) and VGLUT1 (in green). In the insets high magnifications are shown corresponding to the white square areas. Scale bars 20 μm. Left, bar plot summarizes the quantification of VGLUT1 positive puncta, significantly higher in MWCNTs. **(B)** Right, summary graph of the PSCs frequency in standard saline solution and after TTX and Co^{++} application in controls (squares) and MWCNTs (circles). Right, bar plot summarizes the residual activity, in respect to standard saline, after application of TTX and Co^{++}.

(control and MWCNT, respectively). We monitored the synaptic networks before and after cell exposure to MβCD (1 mM; 1 h)[30] by voltage clamp whole-cell recordings, comparing Control neurons with MWCNT ones. The first set of recordings was performed at 8-10 DIV, since at this ages neuronal circuits were reported to display a significant increase in synaptic activity when cultured on MWCNTs.[12,14,15] Figure 2 illustrates this characteristic enhancement in spontaneous synaptic activity brought about by MWCNTs and expressed as a significant ($P < 0.05$) increase (by 133%) in the post synaptic current (PSC) frequency (box plot in Figure 2, *B*, top; control, n = 22; MWCNT, n = 21), leaving PSC amplitudes unperturbed (box plot in Figure 2, *B*, bottom).[12,14,15] Sample tracings of control and MWCNT recordings are shown in Figure 2, *A* (top row).

Exposure to MβCD did not affect neuronal viability and the overall integrity of membranes as estimated by comparing the input resistance values of the recorded neurons before and after treatment (for control: 655 ± 73 MΩ, n = 21, and 694 ± 167 MΩ, n = 23, $P = 0.834$; for MWCNT 487 ± 37 MΩ, n = 22, and 625 ± 90 MΩ, n = 23, $P = 0.117$; prior and after MβCD incubation, respectively) and the values for the cell capacitance (for control: 75 ± 32 pF, n = 21, and 80 ± 7 pF, n = 23, $P = 0.536$; for MWCNT 92 ± 8 pF, n = 22, and 74 ± 7 pF, n = 23,$P = 0.120$; prior and after MβCD incubation, respectively).

Synaptic cholesterol balances spontaneous and evoked neurotransmission by inhibiting spontaneous vesicle turnover and, conversely, by promoting evoked exo-endocytosis.[28] In hippocampal cultures, MβCD-mediated removal of cholesterol has been reported to result in an augmentation of spontaneous synaptic vesicle fusion and recycling.[28]

We measured synaptic activity in these two groups of cultures after cholesterol depletion and, surprisingly, addition of MβCD resulted in two macroscopic, but opposite, changes, illustrated by the sample recordings in Figure 2, *A* (bottom tracings). In control neurons MβCD treatment led to a significant ($P < 0.01$) increase (by 228%) in PSC frequency, without affecting PSC amplitude values; in MWCNTs, on the contrary, MβCD incubation induced a significant reduction in both PSC frequency (by 62%; $P < 0.05$) and PSC amplitude (by 55% $P < 0.01$; summarized in the box plots of Figure 2, *B*). Before analyzing in more details these synaptic changes (see below) we ascertain whether the tight interfacing[14] of neuronal membrane with MWCNTs modulated membrane cholesterol in cultured neurons. Figure 3, *A* shows sample micrographs of cultured neurons (control and MWCNTs) labeled with filipin, used to detect free cholesterol.[41] Cholesterol levels, as measured by filipin fluorescence intensity (see Methods) were similar in the two culture groups (summarized in Figure 3, *A* and *B*). MβCD incubation efficiently removed membrane cholesterol in both culture groups, as documented by the drop in filipin fluorescence intensity after treatments (reduced by 44% in controls and by 52%, in MWCNT, quantified in Figure 3, *B*; n = 30 fields in control and MWCNTs). We further explored the ability of MβCD incubation in altering, in the two neuronal cultures, the integrity of cholesterol/sphingolipid micro-domains (i.e. lipid rafts), expressed by cultured hippocampal neurons.[42] We visualized lipid rafts by double labeling neurons with the raft marker CT-B[43] and the neuronal marker β-tubulin III (Figure 3, *C*). We calculated by confocal analysis the CT-B volume relative to the β-tubulin III one (see Methods) to quantify lipid rafts before and after MβCD incubation. In Figure 3, *C* the bar plot shows the comparable values of the CT-B/β-tubulin III volumes in the two cultures groups, and that apparently MβCD treatment did not deplete CT-B domains in control and MWCNTs. Thus, the used incubation protocol for cholesterol depletion efficiently reduces free cholesterol from neuronal membranes in both cultures, without affecting the integrity of cholesterol-enriched structures, such as lipid rafts.

Despite the similar effects with respect to cholesterol, MβCD affects in an opposite manner PSCs frequency in control and MWCNTs, suggesting the presence of presynaptic terminals where vesicle release is differentially regulated by cholesterol.[44]

Effects of acute cholesterol depletion on glutamatergic synapses

Spontaneous synaptic activity in our recording conditions[15] was manifested as inward currents made up by a mixed population of inhibitory ($GABA_A$-receptor mediated) and

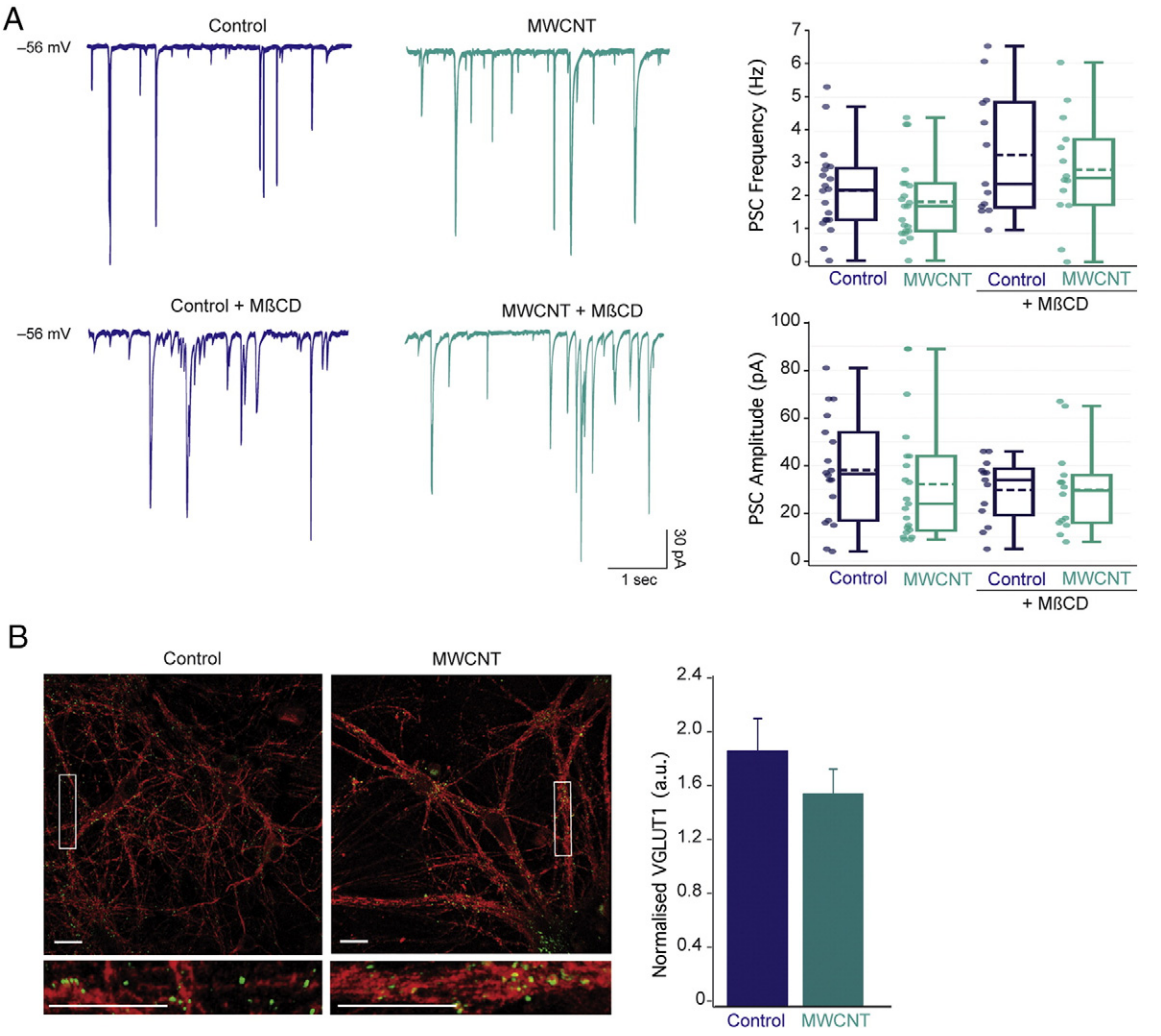

Figure 6. Controls and MWCNTs spontaneous synaptic activity in long-term cultures. **(A)** Left, representative recordings of synaptic activity at 21 DIV in controls and MWCNTs before (top) and after (bottom) MβCD. Box plots (right) summarize the values of PSCs frequency (top) and amplitude (bottom); note the similar values measured in all conditions. **(B)** Confocal micrographs of cultures labeled by β-tubulin III (in red) and VGLUT1 (in green). In the insets high magnifications are shown corresponding to the white square areas. In long-term cultures controls and MWCNTs neurons display similar amount of VGLUT1 puncta, summarized in the bar plot (right). Scale bar, 20 μm.

excitatory (glutamate AMPA-receptor mediated) PSCs, characterized by different kinetics.[15] To gain insights into the MβCD regulation of synaptic activity in the two culture groups, we randomly selected a subset of control (n = 7) and MWCNT (n = 7) neurons to perform offline differential analysis of PSCs kinetic, in particular of their decay.[12,45] By means of their kinetic properties we identified slow decaying PSCs (τ = 22.0 ± 2.0 ms in control; τ = 21.2 ± 1.1 ms in MWCNTs; Figure 4, *A* top right) corresponding to $GABA_A$ receptor-mediated events from fast decaying (τ = 3.1 ± 0.3 ms in control; τ = 3.4 ± 0.4 ms in MWCNTs; Figure 4, *A* top left) events usually corresponding to AMPA-receptor mediated currents.[12,15] The frequency of fast PSCs was upregulated by MβCD in control, but strongly reduced in MWCNT exposed to similar treatments (plot in Figure 4, *A*). Notably, slow PSC frequencies were similarly (and only slightly) reduced in both culture groups when exposed to MβCD.

Cholesterol depletion in neurons is known to increase the rate of spontaneous transmission but it impairs evoked neurotransmission[28,29] and synapses usually segregate, at the presynaptic terminals, the distinct vesicle pools responsible for spontaneous or evoked release.[29,46]

We characterized the effects of cholesterol depletion on spontaneous release by recording miniature PSCs (mPSCs) in the presence of TTX (1 μM). mPSCs, in dissociated hippocampal cultures at this age, comprise virtually only fast events (τ = 4.5 ± 0.6 ms in control, n = 9, and τ = 5 ± 0.9 ms in MWCNT, n = 9; Figure 4, *B*, top tracings) thus representing only excitatory mPSCs.[15] MWCNT mPSCs display, in standard conditions, a significantly ($P < 0.05$) higher frequency (Figure 4, *B*), due to the synaptogenic impact of MWCNTs.[15] The increased number of synapses is further supported in Figure 5, *A* where VGLUT1 labeled presynaptic boutons in β-tubulin III identified neuronal bodies and dendrites, allowed to quantify VGLUT1-positive

puncta, indicating a significant ($P < 0.05$) increase in their density in MWCNT neurons when compared to control ones. MβCD incubation significantly ($P < 0.05$) increased fast mPSCs frequency in control while in MWCNT the frequency of fast minies was only slightly, but not significantly, reduced (plot in Figure 4, *B*); to note, mPSCs amplitudes were not affected by any treatment (box plot in Figure 4, *B*) indicating that the properties of postsynaptic glutamate receptors were not altered by these manipulations.[28]

These results suggest that control and MWCNTs glutamatergic synapses express different release machineries. Namely, control glutamatergic synapses are dominated by spontaneous fusions, on the contrary MWCNT ones preferentially release neurotransmitter in response to action potentials.

To address the expression of heterogeneous populations of presynaptic vesicles, and the different partitioning of synaptic vesicles between the two pools, we estimate the residual activity when PSCs were recorded prior and after the application of TTX and Co^{++} (3 mM; n = 7 control and n = 7 MWCNTs). The block of voltage-gated Ca^{++}-channels impairs the fusion of calcium-dependent vesicles,[47] isolating the calcium-independent "resting pool",[48] mostly involved in spontaneous neurotransmission, namely the component increased by cholesterol removal.[28] In the presence of Co^{++} mPSCs displayed a similar frequency in control and MWCNTs, thus the residual activity in the presence of Ca^{++} channels block, in MWCNTs was significantly smaller ($P < 0.05$; plots in Figure 5, *B*).

This different ratio suggests that synapses in control cultures rely for their basal activity mostly on low calcium-dependent vesicle release.[25]

The effects of acute cholesterol removal in control and MWCNT hippocampal cultures at later stages of synaptic development

Action potential evoked and spontaneous neurotransmitter release modalities involve different molecular machineries regulating segregated vesicle pools at the presynaptic site. Distinct forms of neurotransmission, involving these two modes of release, were reported to change during hippocampal synaptic development in vitro.[49] Immature synapses display high levels of spontaneous release with respect to more mature neurons where evoked release became particularly strong.[49] Indeed, in our experiments the acute removal of cholesterol unmasked an opposite vesicle homeostasis across control and MWCNTs, hinting at a tuning of synaptic maturation.[49] To investigate whether the different synaptic responses to MβCD between control and MWCNTs were related to a transient unbalance toward more mature release phenotype in the newly formed MWCNT synapses, we extended our investigation to neurons in control (n = 20) or interfaced to MWCNTs (n = 22) recorded at 18-21 DIV. In older cultures, the frequency of MWCNT PSCs did not differ from that measured at earlier stages of development under the same growth conditions (compare plots in Figure 2, *B* and in Figure 6, *A*), and was similar to the value measured in aged-matched control neurons, which conversely increased the frequency of PSCs upon in vitro development. Figure 6, *A* shows sample recordings (left) with the pooled values for PSC frequency and amplitude summarized in the box plots (right). The comparable control and MWCNT synaptic activity, suggested by the similar PSC frequency, was supported by immunofluorescence quantification of VGLUT1-positive puncta. As shown in Figure 6, *B* we detected a similar density of positive puncta between the two culture groups. Also in these measures, MWCNT values were equal to those detected at earlier stages of development (compare plots in Figures 5, *A* and 6, *B*), while in control an age dependent increase in puncta was evident. In accordance to these measures, Figure S1A shows that frequency and amplitude of mPSCs did not differ when comparing control and MWCNT at 18-21 DIV.

At 18-21 DIV incubating with MβCD induced a slight and non-significant increase (Figure 6A) in the frequency of PSCs in both cultures groups, without altering PSCs amplitudes, suggesting that in vitro aging leads to an overall balance between synapses expressing different release modes.[49] During the development of hippocampal neurons in culture, the levels of membrane cholesterol usually increase[50] thus we tested the ability of MβCD incubation in depleting cholesterol in 18-21 DIV neurons. Supplemental Figure S1, *B* shows the reduction in filipin fluorescence after MβCD incubation, supporting the efficacy of such a treatment.

These results strengthen the hypothesis that MWCNTs boost the overall network maturation, in terms of number of synapses and efficacy,[15] but in the long-term these effects reach a steady state, probably due to the maximal connectivity homeostatically set by the size of any given neuronal network.[51]

Discussion

Carbon nanotubes are increasingly incorporated in the development of novel two-dimensional biomaterials designed to interface tissue reconstruction and signaling.[16,52] In material science, MWCNTs are adopted in composites to strengthen biomaterial mechanical properties, electrical conductivity or microenvironment-defining moieties.[53] However, MWCNTs are not inert and promote synaptogenesis when interfaced to cultured neurons.[15,54] In the present study we used dissociated cultures to investigate MWCNT ability to alter membrane lipid homeostasis to pinpoint the earliest mechanisms that may contribute in modulating synaptic activity. We also characterized to what extent the MWCNTs driven synaptic enhancement is maintained throughout long-term network development.

The principal finding of the present report is that two-dimensional MWCNT interfaces do not alter the homeostasis of membrane lipids, in particular cholesterol, in neurons. In fact, neurons cultured interfaced to MWCNTs, display a similar membrane cholesterol distribution and, when we used a traditional tool to remove membrane cholesterol, MβCD,[26] this treatment was as effective as in control cells. This result differs from our preliminary observations on artificial lipid membranes, excluding, in living neurons, a decrease mobility of the lipid molecules via preferential interactions with the carbon nanotubes.[21] In this work we confirm the notion that MWCNT microenvironment provide cues instructing the construction of more synapses[15,54] documented by the increase in PSCs frequency, in mPSCs and in VGLUT1-positive labeling; the

latter showing, for the first time directly by confocal microscopy, the higher density of glutamatergic synapses.[15]

The present data show that, in both culture groups, the treatment used to remove cholesterol did not affect cell viability, as sustained by the values of cell input resistance and membrane capacitance.[55,56] In addition, membrane micro-domains enriched in cholesterol such as lipid rafts,[57] involved in the regulation of ionotropic glutamate receptor function,[42] displayed a similar distribution in control and MWCNT neurons when investigated by immunofluorescence labeling and confocal microscopy[58]; these structures where not altered by MβCD treatments and indeed, in both cultures groups, miniature events' analysis suggested the absence of major post synaptic changes due to cholesterol removal.[28]

However, we found that at 8-10 DIV, release at glutamatergic synapses in control and MWCNTs was regulated in an opposite manner by cholesterol reduction.

To understand the reason for the observed difference, we examined the main variable that might conceivably affect release tuning by cholesterol. We had already excluded the possibility of differences in membrane cholesterol distribution and depletion. We thus turned our attention to pre-synaptic process that may be regulated by cholesterol. Removal of cholesterol variably affects spontaneous or evoked neurotransmitter release in cultured neurons, improving spontaneous vesicle fusion and decreasing evoked vesicle recycling.[28]

We thus hypothesized that control synapses display a higher relative amount of spontaneous vesicle pools with respect to MWCNT ones.

In the presence of TTX we observed that in control conditions the frequency of mPSCs was still affected by MβCD, whereas no changes occurred in MWCNT neurons. Our hypothesis was further supported by the block of voltage dependent Ca^{++}-channels by Co^{++} applications.[59] This condition indicated the presence of an opposite ratio between high and low Ca^{++}-dependent vesicle pools in control and MWCNT presynaptic glutamatergic terminals.

Recent reports have shown that the maturation of neurotransmission is accompanied by changes in pre-synaptic release modes; in particular spontaneous vesicle pools are predominant on evoked ones during early stages of development, and these two populations are gradually rebalanced during the synaptic maturation process.[49,60]

It is tempting to speculate that MWCNTs accelerate synaptic network maturation, improving synapse formation and favoring more mature release modes, an effect that is homeostatically regulated upon prolonged interfacing. In fact, in our experiments, control and MWCNTs displayed functional and anatomical similarities after three weeks of growth. We cannot distinguish whether this was due to a progressive shielding of the MWCNTs by extracellular matrix proteins,[61] thus changing the nano-bio interface, or rather by the homeostatic regulation of cultured neuronal networks, constraining the maximal number of synapses[51] and their level of maturation in vitro.

In conclusion, the main finding of the present study is that MWCNTs when used in interfacing neurons can regulate synapse formation and function in a dynamic manner, tuning exquisite neurobiological mechanisms, such as neuronal maturation.[62] This ability is however controlled and limited by the physiological maturation of the synaptic circuit. This functional integration of the MWCNTs within the newly formed neuronal network might represent an attractive property in designing interfaces for neuronal repair.

Brain interfaces of the future require the application of nanomaterial-related technologies to target some of the current ambitions in interfacing neurons: improving the stability, flexibility and durability of the interface, improving the efficacy of the charge transfer to and from neurons, and minimizing the reactivity in the surrounding tissue.[63] The aim is that of realizing high resolution and minimally invasive interfaces between recording probes and biological systems,[64] able to map brain activity and deliver precise stimuli, to interface the brain to an external device or to facilitate recovery of function via engaging neuronal plasticity processes,[65] eventually interfacing the brain to the spinal cord, to regain motor function after spinal cord lesions.[66] In this arena, conductive nano-materials such as carbon nanotubes may be the adequate response to reach miniaturization of the electrodes and neuronal-scale stimulation and recordings, leading to an improved merging between electronic and biosystems.[67] We recently reported low tissue reaction upon implantation in vivo of unmodified MWCNT microsystems, suggesting a biocompatibility crucial to further design of miniaturized platforms based on entirely new materials.[17]

Appendix A. Supplementary data

Supplementary data to this article can be found online at http://dx.doi.org/10.1016/j.nano.2017.01.020.

References

1. Lutolf MP, Hubbell JA. Synthetic biomaterials as instructive extracellular microenvironments for morphogenesis in tissue engineering. *Nat Biotechnol* 2005;**23**:47-55.
2. Dvir T, Timko BP, Kohane DS, Langer R. Nanotechnological strategies for engineering complex tissues. *Nat Nanotechnol* 2011;**6**:13-22.
3. Shao Y, Fu J. Integrated micro/nanoengineered functional biomaterials for cell mechanics and mechanobiology: a materials perspective. *Adv Mater* 2014;**26**:1494-533.
4. Battiston KG, Cheung JW, Jain D, Santerre JP. Biomaterials in co-culture systems: towards optimizing tissue integration and cell signaling within scaffolds. *Biomaterials* 2014;**35**:4465-76.
5. Zhu W, O'Brien C, O'Brien JR, Zhang LG. 3D nano/microfabrication techniques and nanobiomaterials for neural tissue regeneration. *Nanomedicine (Lond)* 2014;**9**:859-75.
6. Seidlits SK, Lee JY, Schmidt CE. Nanostructured scaffolds for neural applications. *Nanomedicine (Lond)* 2008;**3**:183-99.
7. Tian B, Liu J, Dvir T, Jin L, Tsui JH, Qing Q, et al. Macroporous nanowire nanoelectronic scaffolds for synthetic tissues. *Nat Mater* 2012;**11**:986-94.
8. Kotov NA, Winter JO, Clements IP, Jan E, Timko EP, Campidelli S, et al. Nanomaterials for neural interfaces. *Adv Mater* 2009;**21**:3970-4004.
9. Marchesan S, Melchionna M, Prato M. Wire up on carbon nanostructures! How to play a winning game. *ACS Nano* 2015;**9**:9441-50.
10. Mattson MP, Haddon RC, Rao AM. Molecular functionalization of carbon nanotubes and use as substrates for neuronal growth. *J Mol Neurosci* 2000;**14**:175-82.

11. Fabbro A, Villari A, Laishram J, Scaini D, Toma FM, Turco A, et al. Spinal cord explants use carbon nanotube interfaces to enhance neurite outgrowth and to fortify synaptic inputs. *ACS Nano* 2012;**6**:2041-55.
12. Lovat V, Pantarotto D, Lagostena L, Cacciari B, Grandolfo M, Righi M, et al. Carbon nanotube substrates boost neuronal electrical signaling. *Nano Lett* 2005;**5**:1107-10.
13. Mazzatenta A, Giugliano M, Campidelli S, Gambazzi L, Businaro L, Markram H, et al. Interfacing neurons with carbon nanotubes: electrical signal transfer and synaptic stimulation in cultured brain circuits. *J Neurosci* 2007;**27**:6931-6.
14. Cellot G, Cilia E, Cipollone S, Rancic V, Sucapane A, Giordani S, et al. Carbon nanotubes might improve neuronal performance by favouring electrical shortcuts. *Nat Nanotechnol* 2009;**4**:126-33.
15. Cellot G, Toma FM, Varley ZK, Laishram J, Villari A, Quintana M, et al. Carbon nanotube scaffolds tune synaptic strength in cultured neural circuits: novel frontiers in nanomaterial-tissue interactions. *J Neurosci* 2011;**31**:12945-53.
16. Fabbro A, Prato M, Ballerini L. Carbon nanotubes in neuroregeneration and repair. *Adv Drug Deliv Rev* 2013;**65**(15):2034-44.
17. Usmani S, Aurand ER, Medelin M, Fabbro A, Scaini D, Laishram J, et al. 3D meshes of carbon nanotubes guide functional reconnection of segregated spinal explants. *Sci Adv* 2016;**2**(7):e1600087.
18. Nel AE, Mädler L, Velegol D, Xia T, Hoek EM, Somasundaran P, et al. Understanding biophysicochemical interactions at the nano-bio interface. *Nat Mater* 2009;**8**(7):543-57.
19. Lesniak A, Salvati A, Santos-Martinez MJ, Radomski MW, Dawson KA, Åberg C. Nanoparticle adhesion to the cell membrane and its effect on nanoparticle uptake efficiency. *J Am Chem Soc* 2013;**135**(4):1438-44.
20. Wang Y, Yang Y, Yan L, Kwok SY, Li W, Wang Z, et al. Poking cells for efficient vector-free intracellular delivery. *Nat Commun* 2014;**5**:4466.
21. Khanbabaie R, Jahanshahi M. Revolutionary impact of Nanodrug delivery on neuroscience. *Curr Neuropharmacol* 2012;**10**:70-392.
22. Malarkey EB, Reyes RC, Zhao B, Haddon RC, Parpura V. Water soluble single-walled carbon nanotubes inhibit stimulated endocytosis in neurons. *Nano Lett* 2008;**8**:3538-42.
23. Aldinucci A, Turco A, Biagioli T, Toma FM, Bani D, Guasti D, et al. Carbon nanotube scaffolds instruct human dendritic cells: modulating immune responses by contacts at the nanoscale. *Nano Lett* 2013;**13**:6098-105.
24. Dayani Y, Malmstadt N. Lipid bilayers covalently anchored to carbon nanotubes. *Langmuir* 2012;**28**:8174-82.
25. Baoukina S, Monticelli L, Tieleman DP. Interaction of pristine and functionalized carbon nanotubes with lipid membranes. *J Phys Chem B* 2013;**117**:12113-23.
26. Lopez CF, Nielsen SO, Moore PB, Klein LM. Understanding nature's design for a nanosyringe. *S A* 2004;**101**:4431-4.
27. Monticelli L, Salonen E, Chun Ke P, Vattulainen I. Effects of carbon nanoparticles on lipid membranes: a molecular simulation perspective. *Soft Matter* 2009;**5**:4433-45.
28. Wasser CR, Ertunc M, Liu X, Kavalali ET. Cholesterol-dependent balance between evoked and spontaneous synaptic vesicle recycling. *J Physiol* 2007;**579**(2):413-29.
29. Ramirez DM, Kavalali ET. Differential regulation of spontaneous and evoked neurotransmitter release at central synapses. *Curr Opin Neurobiol* 2011;**21**:275-82.
30. Zidovetzki R, Levitan I. Use of cyclodextrins to manipulate plasma membrane cholesterol content: evidence, misconceptions and control strategies. *Biochim Biophys Acta* 2007;**1768**:1311-24.
31. Nečas D, Klapetek P. Gwyddion: an open-source software for SPM data analysis. *Phys* 2012;**10**:181-8.
32. Christian AE, Haynes MP, Phillips MC, Rothblat GH. Use of cyclodextrins for manipulating cellular cholesterol content. *J Lipid Res* 1997;**38**:2264-72.
33. Steck TL, Ye J, Lange Y. Probing red cell membrane cholesterol movement with cyclodextrin. *Biophys J* 2002;**83**:2118-25.
34. Hissa B, Duarte JG, Kelles LF, Santos FP, del Puerto HL, Gazzinelli-Guimaraes PH, et al. Membrane cholesterol regulates lysosome-plasma membrane fusion events and modulates Trypanosoma cruzi invasion of host cells. *PLoS Negl Trop Dis* 2012;**6**:e1583.
35. Richter RP, Brisson A. Characterization of lipid bilayers and protein assemblies supported on rough surfaces by atomic force microscopy. *Langmuir* 2003;**19**:1632-40.
36. Stone N, Kendall C, Smith J, Crow P, Barr H. Raman spectroscopy for identification of epithelial cancers. *Faraday Discuss* 2004;**126**:141-57.
37. Bergholt MS, Zheng W, Ho KY, Teh M, Yeoh KG, So JBY, et al. Fiber-optic Raman spectroscopy probes gastric carcinogenesis in vivo at endoscopy. *J Biophotonics* 2013;**6**:49-59.
38. Osswald S, Havel M, Gogotsi Y. Monitoring oxidation of multiwalled carbon nanotubes by Raman spectroscopy. *J Raman Spectrosc* 2007;**38**:728-36.
39. Lehman JH, Terrones M, Mansfield E, Hurst KE, Meunier V. Evaluating the characteristics of multiwall carbon nanotubes. *Carbon* 2011;**49**:2581-602.
40. Lepot L, De Wael K, Gason F, Gilbert B. Application of Raman spectroscopy to forensic fibre cases. *Sci Justice* 2008;**48**:109-17.
41. Fünfschilling U, Jockusch WJ, Sivakumar N, Möbius W, Corthals K, Li S, et al. Critical time window of neuronal cholesterol synthesis during neurite outgrowth. *J Neurosci* 2012;**32**:7632-45.
42. Hering H, Lin CC, Sheng M. Lipid rafts in the maintenance of synapses, dendritic spines, and surface AMPA receptor stability. *J Neurosci* 2003;**23**:3262-71.
43. Blank N, Schiller M, Krienke S, Wabnitz G, Ho AD, Lorenz HM. Cholera toxin binds to lipid rafts but has a limited specificity for ganglioside GM1. *Immunol Cell Biol* 2007;**85**:378-82.
44. Moulder KL, Jiang X, Taylor AA, Shin W, Gillis KD, Mennerick S. Vesicle pool heterogeneity at hippocampal glutamate and GABA synapses. *J Neurosci* 2007;**27**:9846-54.
45. Clements JD, Bekkers JM. Detection of spontaneous synaptic events with an optimally scaled template. *Biophys J* 1997;**73**:220-9.
46. Melom JE, Akbergenova Y, Gavornik JP, Littleton JT. Spontaneous and evoked release are independently regulated at individual active zones. *J Neurosci* 2013;**33**:17253-63.
47. Ermolyuk YS, Alder FG, Surges R, Pavlov IY, Timofeeva Y, Kullmann DM, et al. Differential triggering of spontaneous glutamate release by P/Q-, N- and R-type Ca2+ channels. *Nat Neurosci* 2013;**16**:1754-63.
48. Fredj NB, Burrone J. A resting pool of vesicles is responsible for spontaneous vesicle fusion at the synapse. *Nat Neurosci* 2009;**12**:751-8.
49. Andreae LC, Fredj NB, Burrone J. Independent vesicle pools underlie different modes of release during neuronal development. *J Neurosci* 2012;**32**:1867-74.
50. Nicholson AM, Ferreira A. Increased membrane cholesterol might render mature hippocampal neurons more susceptible to beta-amyloid-induced calpain activation and tau toxicity. *J Neurosci* 2009;**29**:4640-51.
51. Boyer C, Schikorski T, Stevens CF. Comparison of hippocampal dendritic spines in culture and in brain. *Neuroscience* 1998;**18**:5294-300.
52. Harrison BS, Atala A. Carbon nanotube applications for tissue engineering. *Biomaterials* 2007;**28**:344-53.
53. Bosi S, Ballerini L, Prato M. Carbon nanotubes in tissue engineering. *Top Curr Chem* 2014;**348**:181-204.
54. Kim YG, Kim JW, Pyeon HJ, Hyun JK, Hwang JY, Choi SJ, et al. Differential stimulation of neurotrophin release by the biocompatible nano-material (carbon nanotube) in primary cultured neurons. *J Biomater Appl* 2014;**28**:790-7.
55. Carp JS. Physiological properties of primate lumbar Motoneurons. *J Neurophysiol* 1992;**68**:1121-32.
56. Gao Y, Liu L, Li Q, Wang Y. Differential alterations in the morphology and electrophysiology of layer II pyramidal cells in the primary visual cortex of a mouse model prenatally exposed to LPS. *Neurosci Lett* 2015;**591**:138-43.
57. Allen JA, Halverson-Tamboli RA, Rasenick MM. Lipid raft microdomains and neurotransmitter signalling. *Nat Rev Neurosci* 2007;**8**:128-40.
58. Webb RH. Confocal optical microscopy. *Rep Prog Phys* 1996;**59**:427-71.
59. Mitterdorfer J, Bean BP. Potassium currents during the action potential of hippocampal CA3 neurons. *J Neurosci* 2002;**22**:10106-15.

60. Andreae LC, Burrone J. Spontaneous neurotransmitter release shapes dendritic arbors via long-range activation of NMDA receptors. *Cell Rep* 2015;**10**(6):873-82.
61. Barros CS, Franco SJ, Müller U. Extracellular matrix: functions in the nervous system. *Cold Spring Harb Perspect Biol* 2011;**3**:a005108.
62. Fabbro A, Sucapane A, Toma FM, Calura E, Rizzetto L, Carrieri C, et al. Adhesion to carbon nanotube conductive scaffolds forces action-potential appearance in immature rat spinal neurons. *PLoS One* 2013;**8**(8):e73621.
63. Fattahi P, Yang G, Kim G, Abidian MR. A review of organic and inorganic biomaterials for neural interfaces. *Adv Mater* 2014;**26**:1846-85.
64. Duan X, Lieber CM. Nanoelectronics meets biology: from new nanoscale devices for live-cell recording to 3D innervated tissues. *Chem Asian J* 2013;**8**(10):2304-14.
65. Moorjani S. Miniaturized technologies for enhancement of motor plasticity. *Front Bioeng Biotechnol* 2016;**18**(4):30.
66. Capogrosso M, Milekovic T, Borton D, Wagner F, Moraud EM, Mignardot JB, et al. A brain-spine interface alleviating gait deficits after spinal cord injury in primates. *Nature* 2016;**539**:284-8.
67. Vitale F, Summerson SR, Aazhang B, Kemere C, Pasquali M. Neural stimulation and recording with bidirectional, soft carbon nanotube fiber microelectrodes. *ACS Nano* 2015;**9**(4):4465-74.